# The crystal structure of MexR from *Pseudomonas aeruginosa* in complex with its antirepressor ArmR

**Mark S. Wilke*, Markus Heller*, A. Louise Creagh[†‡], Charles A. Haynes[†‡§], Lawrence P. McIntosh*[†§¶], Keith Poole[‖], and Natalie C. J. Strynadka*[†§]****

Departments of *Biochemistry and Molecular Biology, [‡]Chemical and Biological Engineering, and [¶]Chemistry, [†]Michael Smith Laboratories, and [§]Center for Blood Research, University of British Columbia, Vancouver, BC, Canada V6T1Z3; and [‖]Department of Microbiology and Immunology, Queen's University, Kingston, ON, Canada K7L3N6

Edited by Brian W. Matthews, University of Oregon, Eugene, OR, and approved August 8, 2008 (received for review June 5, 2008)

**The intrinsic antimicrobial resistance of the opportunistic human pathogen *Pseudomonas aeruginosa* is compounded in mutant strains that overexpress multidrug efflux pumps such as the prominent drug-proton antiporter, MexAB-OprM. The primary regulator of the *mexAB-oprM* operon is the MarR family repressor, MexR. An additional repressor, NalC, also regulates *mexAB-oprM* by controlling expression of ArmR, an antirepressor peptide that is hypothesized to prevent the binding of MexR to its cognate DNA operator via an allosteric protein–peptide interaction. To better understand how ArmR modulates MexR, we determined the MexR-binding region of ArmR as its C-terminal 25 residues and solved the crystal structure of MexR in a 2:1 complex with this ArmR fragment at 1.8 Å resolution. This structure reveals that the C-terminal residues of ArmR form a kinked $\alpha$-helix, which occupies a pseudo-symmetrical and largely hydrophobic binding cavity located at the centre of the MexR dimer. Although the ArmR-binding cavity partially overlaps with the small molecule effector-binding sites of other MarR family members, it possesses a larger and more complex binding surface to accommodate the greater size and specific physicochemical properties of a peptide effector. Comparison with the structure of apo-MexR reveals that ArmR stabilizes a dramatic conformational change that is incompatible with DNA-binding. Thus, this work defines the structural mechanism by which ArmR allosterically derepresses MexR-controlled gene expression in *P. aeruginosa* and reveals important insights into the regulation of multidrug resistance.**

gene regulation | MarR | mexAB-oprM | PA3719 | protein peptide

Bacterial multidrug efflux pumps confer widespread antibiotic resistance by actively purging their cells of chemically diverse xenobiotics. The opportunistic human pathogen *Pseudomonas aeruginosa* possesses a number of these efflux systems, including at least 10 belonging to the resistance nodulation division (RND) superfamily (1, 2). The intrinsic resistance conferred by these pumps is compounded in *P. aeruginosa* because of a synergy of heightened drug efflux and low outer membrane permeability (3). Composed of three components (an inner membrane drug/proton antiporter, an outer membrane channel, and a periplasmic adapter), RND efflux systems appear to extrude noxious substrates by using a rotating peristaltic pump-like mechanism (4, 5). The best-characterized efflux system in *P. aeruginosa* is MexAB-OprM, which displays an expansive substrate profile that includes not only antibiotics and biocides, but organic solvents, dyes, detergents, and homoserine lactones involved in quorum sensing (3). Although pentachlorophenol exposure appears to up-regulate *mexAB-oprM* (6), expression of these efflux genes is generally considered constitutive in wild-type (WT) strains. However, mutations in any of three regulatory genes, *mexR* (7, 8), *nalC* (9, 10), or *nalD* (11), have been shown to cause hyperexpression of *mexAB-oprM* and increased resistance to various medically relevant antimicrobials (11, 12).

The *mexAB-oprM* operon is primarily regulated by the MarR family repressor, MexR, although the TetR family repressor, NalD, provides additional regulation at a weaker promoter (13). MexR forms a homodimer of 147 aa per subunit (total molecular mass of ≈34 kDa) and recognizes two operator sites that overlap promoters for both *mexR* and *mexAB-oprM* (14, 15). A second TetR family repressor, NalC, indirectly influences *mexAB-oprM* expression by repressing production of ArmR, a 53-aa antirepressor that appears to bind MexR at the exclusion of cognate DNA (9, 16). MexR has been shown to be modulated by a peptide effector, whereas all other MarR family effectors known to date are small hydrophobic (typically phenolic) compounds (17). The signal responsible for alleviating NalC repression in WT *P. aeruginosa* is currently unknown.

The MarR family of transcriptional regulators is widely distributed in bacteria and archaea and control various biological processes, including resistance to antimicrobials, sensing of aromatic xenobiotics, and virulence (18). Whereas MarR proteins are poorly conserved in amino acid sequence, they share a common fold that consists of a helical dimerization domain and two winged helix (or winged helix–turn–helix) DNA-binding domains (19). By conserving structure while varying amino acid sequence, the different members of this family have apparently diverged to recognize a large variety of signaling molecules and DNA targets. The crystal structure of MexR and other MarR family proteins have been determined (19–25), but detailed mechanistic information is currently limited by a paucity of structures of MarR family members in complex with their effectors.

Mutational analysis of MexR suggests that ArmR may act allosterically to competitively prevent DNA binding by interacting with MexR at a separate location from its DNA binding site (16). To better understand how interaction with ArmR alleviates MexR repression of *mexAB-oprM*, we determined the 1.8 Å crystal structure of the MexR double mutant Q106L/A110L ($MexR_{LL}$) in a 2:1 complex with an ArmR fragment containing residues 29–53 ($ArmR_C$). This structure reveals that a single $ArmR_C$ molecule occupies a pseudosymmetrical and largely hydrophobic binding cleft within the center of the $MexR_{LL}$ dimer. This effector binding site is separate from the MexR–DNA interface and partially overlaps with the small molecule

Author contributions: M.S.W. and N.C.J.S. designed research; M.S.W., M.H., and A.L.C. performed research; C.A.H., L.P.M., and K.P. contributed new reagents/analytic tools; M.S.W., M.H., and A.L.C. analyzed data; and M.S.W., L.P.M., K.P., and N.C.J.S. wrote the paper.

The authors declare no conflict of interest.

This article is a PNAS Direct Submission.

Data deposition: The atomic coordinates have been deposited in the Protein Data Bank, www.pdb.org (PDB ID code 3ECH).

**To whom correspondence should be addressed. E-mail: natalie@byron.biochem.ubc.ca.

This article contains supporting information online at www.pnas.org/cgi/content/full/0805489105/DCSupplemental.

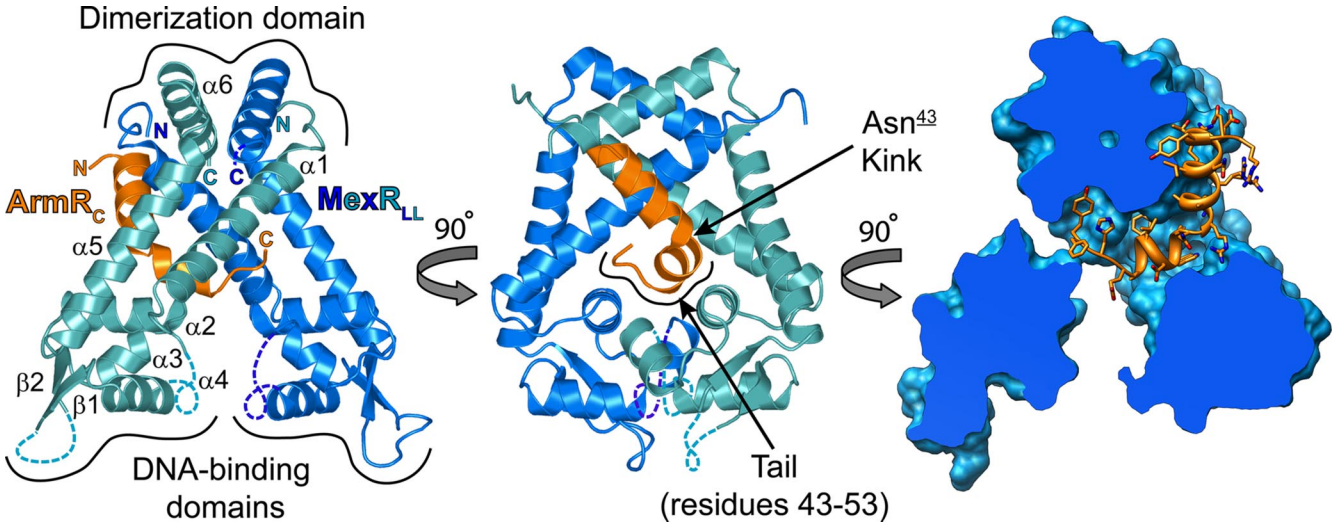


**Fig. 1.** The crystal structure of the MexR$_{LL}$–ArmR$_C$ complex. Cartoon of the MexR$_{LL}$ dimer (blue) in complex with ArmR$_C$ (orange) and cross-section of MexR$_{LL}$ (blue surface) with ArmR$_C$ shown in ribbon and stick representation (C, N and O atoms in orange, blue and red, respectively). Disordered segments are indicated with dashed lines.

effector-binding sites recently identified in other MarR family members. Comparison with the crystal structure of apo-MexR reveals that ArmR stabilizes a tertiary and quaternary conformational change that allosterically repositions the MexR DNA-binding lobes into an orientation that is incompatible with DNA binding. Thus, this structure defines the mechanism by which ArmR allosterically derepresses MexR-controlled gene expression in *P. aeruginosa* and provides important insights into the regulation of multidrug resistance.

## Results and Discussion

**Crystal Structure of the MexR$_{LL}$–ArmR$_C$ Complex at 1.8-Å Resolution.** Initial attempts to crystallize the MexR–ArmR complex produced poor-quality crystals that were recalcitrant to standard optimization. Several strategies were pursued to improve diffraction quality, including truncating both MexR and ArmR, and engineering a hydrophobic crystallization epitope on the surface of MexR to generate additional crystal contacts (26). In our search for better diffracting crystals, we discovered that MexR preferentially protects ArmR residues 29–53 from proteolytic degradation. Analyses by NMR spectroscopy and isothermal titration calorimetry (ITC) revealed that this sequence is predominantly unstructured in isolation, albeit with helical propensity, and binds MexR with the same affinity as full-length ArmR [details provided in supporting information (SI) *Text* and Figs. S1 and S2]. Well ordered crystals were finally obtained after co-crystallization of this ArmR fragment (denoted ArmR$_C$) with MexR$_{LL}$ (MexR truncated by five C-terminal residues and engineered with a Q106L/A110L crystallization epitope). The structure of the MexR$_{LL}$–ArmR$_C$ complex was solved to 1.8-Å resolution by molecular replacement and refined to a $R_{work}/R_{free}$ of 17.6%/22.9%.

**Architecture of the MexR$_{LL}$–ArmR$_C$ Complex.** The structure of MexR closely resembles other members of the MarR family and consists of two winged helix DNA-binding domains, each linked to a helix-rich dimerization domain by a pair of long helices (25). As previously shown by ITC (16), ArmR$_C$ binds MexR$_{LL}$ in a 1:2 stoichiometry (Fig. 1). Consistent with NMR-based secondary structure propensities (see *SI Text* and Fig. S1), bound ArmR$_C$ forms an $\alpha$-helix spanning residues 32–49 with a severe 75° kink at Asn-43 (underlined numbers indicate ArmR$_C$ residues). ArmR$_C$ associates with MexR$_{LL}$ between its DNA-binding and dimerization domains with residues C-terminal to the kink in the ArmR$_C$ helix (the C-terminal tail) buried between the two subunits of the MexR$_{LL}$ dimer. Of the two engineered leucines, only Leu-110 is involved in crystal contacts, forming a hydrophobic patch with His-107 and symmetry-related residues Val-126 and Ala-129. As expected from their native-like DNA and effector binding affinities (Fig. S3), these mutations are distant from both ArmR$_C$ and the DNA-binding domains.

**Interactions between ArmR$_C$ and MexR$_{LL}$.** The high affinity of MexR for ArmR [$K_d$ = 160–290 nM (16)] is reflected in the crystal structure of the MexR$_{LL}$–ArmR$_C$ complex, which reveals an extensive set of interactions focused around the C-terminal tail of ArmR$_C$ (Fig. 2). These interactions are largely hydrophobic and include the aromatic ArmR$_C$ sidechains of Trp-45, Tyr-48, Phe-52, and Tyr-53. Each of these side chains fits into one of four corresponding hydrophobic pockets (respectively denoted *I, II, I′*, and *II′*), which are arranged in a 2-fold symmetrical fashion within the interior of the MexR$_{LL}$ dimer. The *I* and *I′* hydrophobic pockets are comprised of a nearly identical set of residues from monomer chains A and B, respectively, including Ile-24, Leu-28, Pro-37, Val-40, and Met-112. The presence of Leu-28 and Met-112 in the ArmR$_C$ binding pocket explains why the mutation of either of these residues was previously shown to compromise ArmR binding *in vivo* (16). The *II* and *II′* hydrophobic pockets are made up of residues from both chains of MexR$_{LL}$, but likewise share a common set of residues, including Phe-17 from both subunits and Val-20 and Met-14. There are also a number of prominent polar interactions between ArmR$_C$ and MexR$_{LL}$, including 4 hydrogen bonds to the backbone of ArmR$_C$ and 11 hydrogen bonds and salt bridges to ArmR$_C$ side chains. As with the hydrophobic interactions, identical polar residues from both chains of MexR$_{LL}$ are observed making similar interactions with residues in ArmR$_C$. The side-chain imidazole of His-116 hydrogen bonds with the side-chain hydroxyl of Tyr-48 and the side-chain imidazole of His-116′ (where ′ denotes residues from MexR chain B) hydrogen-bonds with the side-chain hydroxyl of Tyr-53. Additionally, the guanidinium group of Arg-21 makes an electrostatic interaction with the side-chain carboxylate of Asp-46 and the guanidinium group of Arg-21′ makes an electrostatic interaction with the backbone carboxylate of the ArmR$_C$ C terminus.

N-terminal to the kink at Asn-43, the ArmR$_C$ helix is amphi-

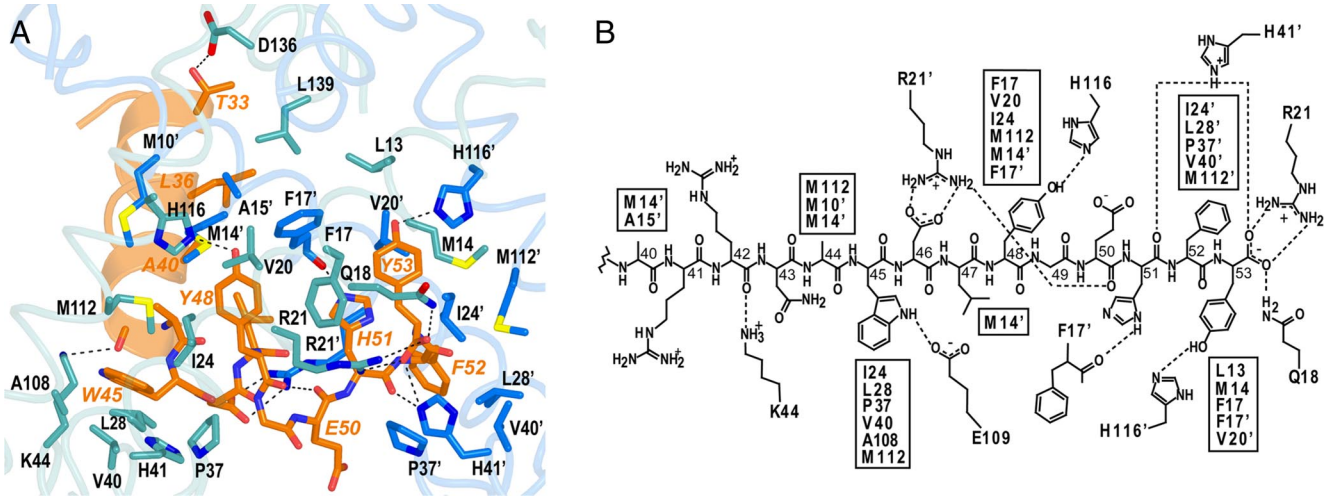


**Fig. 2.** Interactions between $MexR_{LL}$ and $ArmR_C$. (*A*) Stick representation of $ArmR_C$ in its binding site ($MexR_{LL}$ C atoms in blue, $ArmR_C$ C atoms in orange; O, N and S atoms in red, dark blue and yellow, respectively). Hydrogen bonds are shown as dashed lines and $ArmR_C$ labels are italicized and colored orange to distinguish them from $MexR_{LL}$ (black labels; nonprimed, chain A; primed, chain B). (*B*) Schematic map of interactions between $MexR_{LL}$ and residues 40–53 of $ArmR_C$, showing hydrogen bonds and salt bridges by dashed lines. $MexR_{LL}$ residues involved in hydrophobic contacts are listed in boxes.

pathic and associates with the surface of $MexR_{LL}$ via a relatively weak hydrophobic interface. The most prominent interactions in this interface include van der Waal contacts between Leu-36 and MexR residues Leu-139 and Ala-15′ as well as Ala-40 and MexR residues Ala-15′ and Met-14′. In addition, the Thr-33 hydroxyl hydrogen-bonds with the Asp-136 carboxylate and the backbone carbonyl of Arg-42 hydrogen-bonds with Lys-44. The opposite face of the $ArmR_C$ helix is highly charged in this region because of the presence of six arginines, an aspartate, and a glutamate, all of which project their side chains into solvent. Deletion of ArmR residues 1–40 does not compromise MexR binding under ITC conditions (Table S1) and thus the majority of these interactions do not appear to contribute significantly to stabilizing the MexR–ArmR complex.

**Physicochemical Symmetry Within ArmR.** Because of the 2-fold symmetry of the MexR dimer, ArmR can potentially bind MexR in one of two mutually exclusive orientations. As only one complex was observed per asymmetric unit, only one orientation of $ArmR_C$ is observed (at full occupancy and with refined temperature factors similar to MexR). These two sites cannot be occupied simultaneously because they overlap in the interior region of MexR that binds the hydrophobic ArmR tail. This observation not only explains the stoichiometry of the native MexR–ArmR complex, but also reveals a surprising capacity for structural pseudosymmetry in the C-terminal tail of ArmR despite an absence of symmetry in its amino acid sequence. Approximating the two orientations of $ArmR_C$ by swapping the subunits of the $MexR_{LL}$–$ArmR_C$ complex shows that $ArmR_C$ residues Trp-45 and Phe-52 occupy equivalent positions, as do residues Tyr-48 and Tyr-53 (Fig. 3). Consequently, the 2-fold symmetry of the MexR dimer is largely preserved in the resulting complex because of interactions with physicochemically similar aromatic residues in $ArmR_C$. Indeed, the two $MexR_{LL}$ subunits superimposed with rmsd of 1.1 $Å^2$ for all main-chain atoms.

**ArmR-Stabilized Conformational Change.** The intrinsic conformational flexibility of MexR and other members of the MarR family is well established (17). This flexibility is largely caused by the plasticity of loops within the dimerization domain and the hydrophobic nature of the dimerization interface. Moreover, whereas the winged helix DNA-binding domains are relatively rigid entities, the flexibility of the dimerization domain permits various spacing between these two DNA-binding lobes. The previously solved crystal structure of apo-MexR (25) provides an excellent example of this flexibility, displaying four separate conformations of the MexR dimer (denoted AB, CD, EF, and GH) within the asymmetric unit of the crystal. These apo conformations yield inter-DNA domain spacing ranging from 23 to 29 Å (Cα-Cα distance between Arg-73 and Arg-73′, i.e., the middle of the recognition helices α4 and α4′).

An examination of the structure of each apo-MexR dimer reveals that a conformational rearrangement is required to provide sufficient space for the bulky ArmR tail. This necessity is clearly shown by overlapping the dimerization domains of $MexR_{LL}$-$ArmR_C$ and apo-MexR, which reveals that severe steric clashes would occur between $ArmR_C$ and the N-terminal residues of α2 and α2′ if positioned as in apo-MexR (Fig. 4*A*). To accommodate $ArmR_C$-binding, each $MexR_{LL}$ subunit must undergo an α5 bend of ≈20° to move the C terminus of this helix (i.e., Ala-121) by 6–8 Å (depending on the particular apo-MexR dimer used for comparison). In addition, α1 pivots at Thr-22 to displace its N terminus (i.e., Asp-8) by 7–12 Å (Fig. 4*B*). These

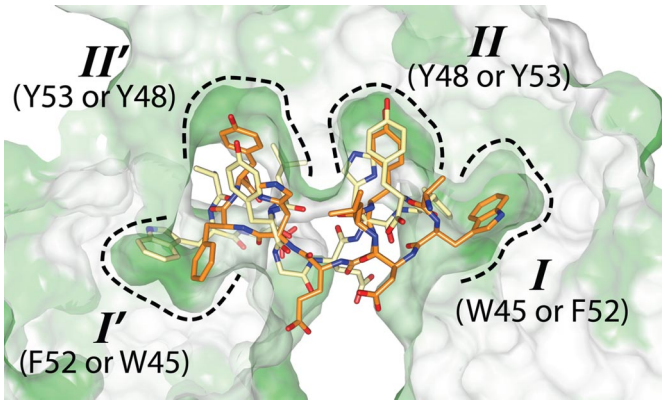


**Fig. 3.** ArmR can bind MexR in two mutually exclusive orientations. Regardless of the orientation, the four hydrophobic pockets of $MexR_{LL}$ (dashed outlines labeled *I*, *II*, *I′* and *II′*) are filled by aromatic $ArmR_C$ residues, revealing physicochemical symmetry within the $ArmR_C$ C terminus. $MexR_{LL}$ is shown as a cross-sectioned hydrophobic surface where green represents relative hydrophobicity.

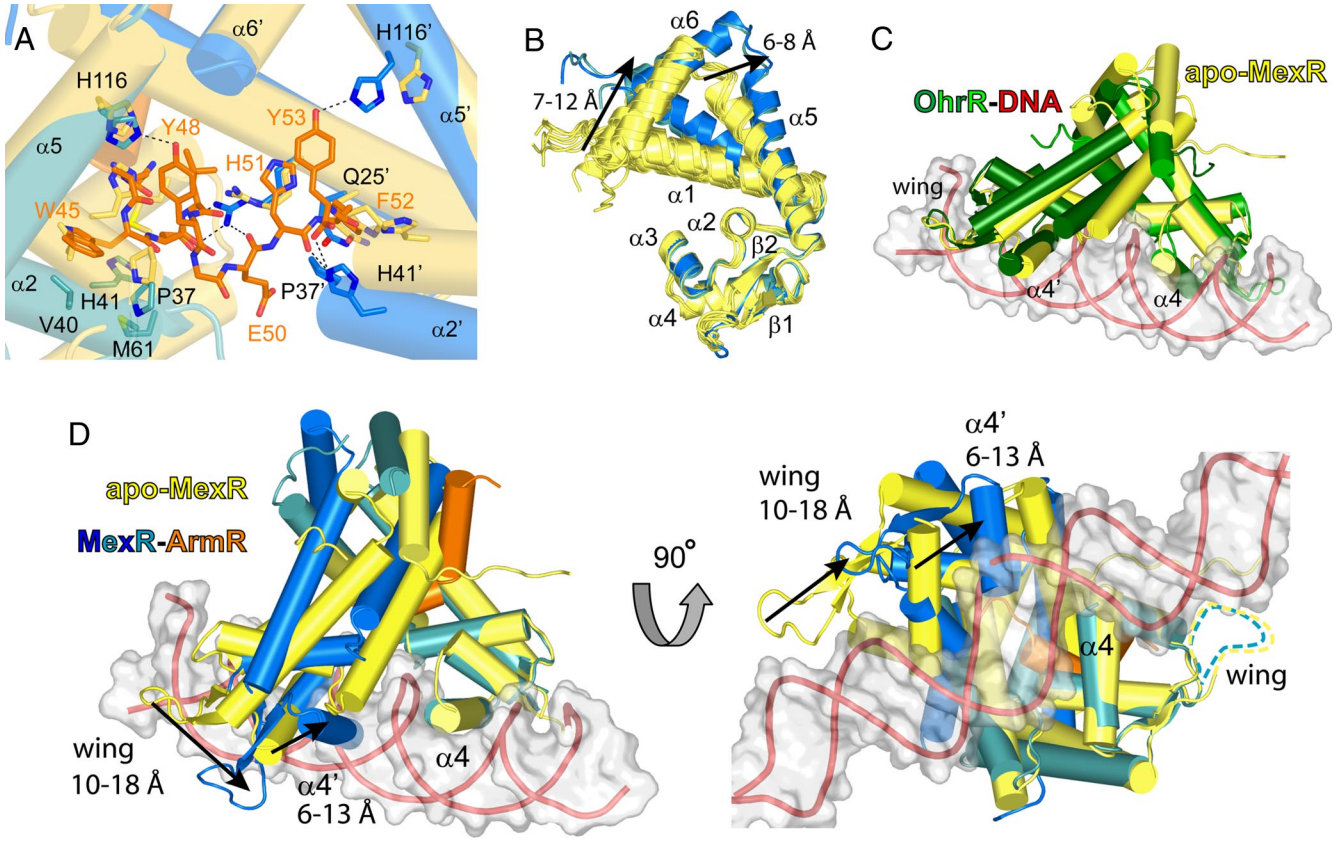


**Fig. 4.** The binding of $ArmR_C$ stabilizes a $MexR_{LL}$ conformation that is incompatible with binding of DNA. (*A*) Steric clashes prevent binding of $ArmR_C$ to apo-MexR, demonstrated by superimposing the dimerization domains of apo-MexR dimer CD (yellow cylinders, PDB ID 1LNW) and $MexR_{LL}$-$ArmR_C$ [blue cylinders with $ArmR_C$ shown as sticks coloured by atom type (C, orange; N, blue; oxygen, red; sulfur, yellow)]. (*B*) Superimposition of the eight chains from the crystal structure of apo-MexR (yellow ribbons) and the two $ArmR_C$-bound $MexR_{LL}$ subunits (blue) reveals the conformational change due to $ArmR_C$ binding. (*C*) Superimposition of the DNA-binding domains of apo-MexR dimer CD (PDB ID 1LNW; yellow cylinders) and DNA-bound OhrR from *Bacillus subtillus* (PDB ID 1Z9C; green cylinders with red ribbons) indicates a highly similar DNA-binding conformation for MexR. (*D*) Superimposing apo-MexR dimer CD (yellow cylinders), as a model for DNA-bound MexR, with the DNA-binding domain of $MexR_{LL}$-$ArmR_C$ (blue and orange cylinders) reveals that the latter cannot bind DNA due to severe steric clashes.

movements increase the distance between the dimerization and the DNA-binding domains of $MexR_{LL}$ and thereby open the *I* and *I′* hydrophobic pockets. Concomitantly, the DNA-binding domains of $ArmR_C$-bound $MexR_{LL}$ twist with respect to the dimerization domain to produce a sheared orientation that shrinks the distance between the N termini of the α4/α4′ recognition helices from 15–20 Å for apo-MexR to 9 Å for the $MexR_{LL}$–$ArmR_C$ complex (Cα-Cα distance between Leu-67 and Leu-67′). These movements displace one domain relative to the other by 10–18 Å for the tip of the wing (i.e., Ser-88) and 6–13 Å for the midpoint of the recognition helix (i.e., Arg[73]; Fig. 4*D*).

**Mechanism of Antirepression.** Of the four conformations available for the apo-MexR dimer, the widest spacing between the DNA-binding lobes was observed in dimer CD (Cα-Cα distance of 29 Å between Arg-73 and Arg-73′). Considering the spacing between major grooves in regular B-DNA is similar (34 Å), it was previously proposed that apo-MexR dimer CD resembles the DNA-bound conformation of MexR (25). Additionally, the shortest spacing was observed in dimer AB (Cα-Cα distance of 23 Å between Arg-73 and Arg-73′), which was found to bind the C-terminal residues of another MexR molecule in the asymmetric unit. Based on these observations, it was speculated that a protein or peptide effector could modify the spacing of the DNA-binding domains and thereby regulate *mexAB-oprM* expression by preventing binding of MexR to its cognate DNA (25). It is now clear that the effector binding site predicted from the AB dimer of apo-MexR partially overlaps with the experimentally observed ArmR binding cleft. The side chains of Asp-146 and Ile-147 from the apo-MexR C terminus appear to reasonably mimic the backbone carboxylate and side chain of the $ArmR_C$ C terminus (i.e., Phe-53). Despite these common interactions, however, the DNA-binding domains of apo-MexR dimer AB did not adopt the sheared orientation that we observe in the $MexR_{LL}$–$ArmR_C$ complex.

Currently, the only structure of a MarR family member in complex with its cognate DNA is OhrR from *Bacillus subtilis* [BsOhrR (23)]. The binding of BsOhrR to its pseudopalindromic DNA operator was shown to induce a global bend of 10° and a slight under-twisting of the otherwise regular B-form DNA. These conformational changes shorten the spacing requirement between the DNA-binding lobes of BsOhrR from 34 Å (to fit regular B-DNA) to 31 Å (Cα-Cα distance between Lys-76 and Lys-76′). In fact, similar protein-induced DNA conformational changes may be typical of the MarR family, as suggested by studies using atomic force microscopy with ExpG (27) and circular dichroism spectroscopy with HucR (28). These studies support the proposal that apo-MexR dimer CD may closely resemble the DNA-bound conformation. Indeed, a comparison of the structures for apo-MexR dimer CD and DNA-bound BsOhrR (Protein Data Bank ID code 1Z9C) reveals that the orientation of their DNA-binding lobes is highly similar (rmsd of

2.2 Å$^2$ for MexR C$\alpha$ atoms corresponding to DNA-binding residues 37–99; Fig. 4*C*). This conclusion is consistent with the structures of reduced apo-OhrR from *Xanthomonas campestris* [XcOhrR (20)], HucR (21), and ST1710 (22), all of which have been observed in conformations that are preconfigured for DNA binding.

Using the structures of $MexR_{LL}$–$ArmR_C$ and apo-MexR dimer CD as models for the effector- and DNA-bound states of MexR, respectively, an allosteric mechanism for the antirepression of MexR can now be proposed. The C-terminal tail of ArmR binds into a cavity between MexR subunits and stabilizes a sheared orientation of the DNA-binding lobes. Superimposition of one DNA-binding domain from apo-MexR dimer CD with the $MexR_{LL}$–$ArmR_C$ complex reveals a displacement of the $\alpha4'$ recognition helix by 13 Å (measured from the C$\alpha$ of Arg-73′), which would result in severe steric clashes with the DNA backbone (Fig. 4 and Movie S1). Moreover, the DNA-binding wing is displaced by as much as 18 Å (measured from the C$\alpha$ of Ser-88′) from its likely position in the DNA minor groove. The wings of BsOhrR were observed making numerous minor groove interactions in the crystal structure of DNA-bound BsOhrR (23), and mutational analysis has established the importance of MexR wing residues Arg-83 and Arg-91 to DNA binding (29). Finally, Glu-50 of bound $ArmR_C$ projects into the gap between the two MexR DNA-binding domains, which places a negatively charged carboxylate group in close proximity to the helix–helix motif, a third DNA-binding element identified in the BsOhrR-DNA structure that primarily uses positively charged residues to bind the negatively charged DNA backbone. As such, we predict Glu-50 is specifically positioned to provide electrostatic repulsion of the DNA backbone in this region, further weakening the affinity of the MexR repressor for its cognate DNA. Taken together, these features define an allosteric mechanism of MexR regulation in which ArmR and DNA binding is mutually exclusive, in accordance with the absence of a ternary complex after combination of MexR, ArmR, and cognate DNA (16).

**Comparison with Other MarR Family Members.** To date, MexR is the only MarR family member known to bind a peptide effector. The ligands for the remaining MarR family members are lipophilic (typically phenolic) compounds such as salicylate or uric acid (17). In several cases, these lipophenolic effectors are organic hydroperoxides that induce structural changes through cysteine oxidation. For example, the crystal structures of reduced and oxidized XcOhrR recently revealed that a nearly perpendicular arrangement of the DNA-binding lobes results from the formation of two intersubunit disulfide bonds (20). This oxidized conformation bears no resemblance to the sheared orientation of the $MexR_{LL}$–$ArmR_C$ complex despite the fact that the oxidizable XcOhrR cysteines occupy locations that are proximal to several elements of the ArmR-binding site in MexR. A number of other MarR family members, such as BsOhrR and MgrA, contain a single oxidizable cysteine and are unlikely to form disulfide bonds (23, 30). The oxidized conformation of these MarR family members remains to be determined, but without added stabilization from disulfides, the perpendicular orientation of XcOhrR is highly unlikely (20). Instead, overoxidation of the reactive cysteine or the formation of either cyclic sulfenamides or protein-effector mixed disulfides (31) is expected to stabilize rearrangements of the DNA-binding lobes, potentially via an ArmR-like mechanism involving steric clashes with residues residing between the dimerization and DNA-binding domains.

The majority of MarR family members, such as MexR, MarR, and HucR, do not contain oxidizable cysteines and are instead regulated by the noncovalent binding of low molecular weight ligands. In the first structure of a MarR family member, salicylate (cocrystallized with MexR at a high concentration of 250 mM) was observed bound to *Escherichia coli* MarR in two sites (SAL-A and SAL-B) positioned on either side of the $\alpha4$ recognition helix (19). This structure suggested a mode of regulation in which DNA-binding is prevented by steric occlusion of the DNA–protein interface. However, the physiological significance of either effector binding site could not be confirmed because the SAL-A salicylate was involved in crystal contacts and the SAL-B salicylate was highly solvent-exposed. Interestingly, the conformation of MarR in the MarR–salicylate crystal structure closely matches that of $MexR_{LL}$–$ArmR_C$, superimposing to 2.8 Å$^2$ rmsd (for 225 common C$\alpha$ residues). This similarity includes not only the relative positions of the recognition helices, but also much of the cavity corresponding to the ArmR binding site. Despite a lack of conserved residues in this region, the presence of a cavity indicates a potential effector binding site. Indeed, recent structures of a MarR family member from *Methanobacterium thermoautotrophicum*, MTH313, revealed two unique salicylate binding sites, one of which corresponds to the oxidizable cysteine (i.e., Cys-15) in BsOhrR (24). These binding sites appear to be mutually exclusive between the two subunits of the MTH313 dimer, producing an asymmetrical conformational change that enlarged the spacing of the DNA-binding lobes relative to apo-MTH313. From these data, it was postulated that the apo form of MTH313 (with narrow spacing) represents the "active" conformation (capable of DNA binding) and the salicylate-bound structure (with wide spacing) represents the "inactive" conformation (incapable of DNA binding). These conclusions are puzzling as they contradict the wide spacing observed in the structure of DNA-bound BsOhrR (23). In fact, the salicylate-bound MTH313 structure appears well configured for DNA binding, superimposing with the structure of DNA-bound BsOhrR to 2.3 Å$^2$ rmsd (for 238 common C$\alpha$ residues). Moreover, the salicylate-bound *E. coli* MarR structure is clearly ill suited for binding a DNA double helix as its DNA-binding lobes share an orientation that is similar to that of the $MexR_{LL}$–$ArmR_C$ complex and its DNA recognition helices are even linked by a pair of salt bridges (19). Regardless, one of the MTH313 salicylate-binding sites appears to partially overlap with the $ArmR_C$-binding site of $MexR_{LL}$, occupying a small pocket between the $\alpha1$ and $\alpha2'$ helices. This position situates salicylate directly between the dimerization and DNA-binding domains of MTH313, in a location that is proximal to the *I*/*I*′ hydrophobic pockets of $MexR_{LL}$ and the oxidizable cysteines of OhrR and MgrA. In contrast to the MTH313 salicylate-binding sites, $MexR_{LL}$ possesses a larger and more complex binding surface to accommodate the greater size and specific physicochemical properties of a peptide effector. Despite these differences, the various members of the MarR family appear to share a similarly positioned effector-binding cavity, suggesting that the MarR family may possess significant mechanistic similarities as well.

The structure of $MexR_{LL}$ in complex with $ArmR_C$ reveals the allosteric mechanism responsible for derepressing production of MexAB–OprM, the major multidrug efflux pump in *P. aeruginosa*. This structure also adds to our understanding of an important family of bacterial transcriptional regulators, many members of which are involved in antimicrobial resistance and virulence. Such knowledge may prove vital in controlling the rise in drug-resistant bacterial infections.

## Materials and Methods

**Protein Production.** The $MexR_{LL}$–$ArmR_C$ complex was produced by coexpression of $MexR_{LL}$ [vector pET41a (Novagen), MexR residues 1–142 with point mutations Q106L and A110L] and $ArmR_C$ [vector pTYB12 (New England Biolabs), ArmR residues 29–53 (i.e., ARRDYTEQLRRAARRNAWDLYGEHFY)] in BL21 Star (DE3) *E. coli* (Invitrogen). The intact complex was purified via three chromatographic steps: (*i*) chitin affinity/intein tag cleavage (New England Biolabs), (*ii*) Mono-Q anion exchange (Amersham Biosciences), and (*iii*) superdex-75 gel filtration (GE Healthcare). Using an Amicon Ultra-15 5K concentrator (Millipore), the pure complex (in 20 mM Tris·HCl, 150 mM NaCl, 5 mM TCEP-HCl, pH 7.5) was concentrated to 9.4 mg/ml as estimated with a predicted $\varepsilon_{280}$ = 12,950 $M^{-1}\cdot cm^{-1}$ (33). More details are provided in *SI Text*.

**Crystallization and Structure Determination.** Crystals of the $MexR_{LL}$–$ArmR_C$ complex were obtained by screening 480 microbatch conditions at 8°C and 18°C by using the Oryx 6 Crystallization Robot (Douglas Instruments). The highest quality crystals grew as clusters from a mixture of 0.5 $\mu$l of protein at 5 mg/ml and 0.5 $\mu$l of 20% (wt/vol) PEG 3000, 0.1 M sodium citrate (pH 5.5) after 2 days under paraffin oil at 18°C. Single crystals were separated, cryoprotected in 20% (wt/vol) PEG 3000, 10% (wt/vol) PEG 1000, and 0.1 M sodium citrate (pH 5.6) and flash-frozen in $N_2(l)$.

Data were collected to 1.8 Å at beamline 8.2.2 of the Advance Light Source (Berkeley, CA) and processed with the program HKL2000 (34). Despite the dramatic conformational differences between apo-MexR and the $MexR_{LL}$–$ArmR_C$ complex, the structure was successfully phased by molecular replacement. To accomplish this, it was necessary to use only the dimerization domain of apo-MexR (residues 3–31 and 105–139) as an initial search model in the program Phaser (35). The position of the dimerization domain was then fixed and the DNA-binding domain (residues 35–98) was used as a search model in the program Molrep (36). The structure was built by using the program Coot (37) and refined by using the programs Phenix (38) and Refmac (39) with a final $R/R_{free}$ of 17.6%/22.9%, respectively. Data collection and refinement statistics are given in Table S2. Graphics were prepared with Pymol (40) and Chimera (41).

**ACKNOWLEDGMENTS.** We thank Dr. Raz Zarivach for assistance with x-ray data collection and the U.S. Department of Energy and the Advanced Light Source (Berkeley, CA) for access to beamline 8.2.2. The work was funded by the Howard Hughes Medical Institute, Canadian Institutes of Health Research, Michael Smith Foundation for Health Research, Canadian Foundation for Innovation, and the University of British Columbia Blusson Fund. M.S.W. was supported by the Canadian Institutes of Health Research and the Michael Smith Foundation for Health Research. M.H. was supported by the Alexander von Humboldt Foundation.

1. Mima T, Sekiya H, Mizushima T, Kuroda T, Tsuchiya T (2005) Gene cloning and properties of the RND-type multidrug efflux pumps MexPQ-OpmE and MexMN-OprM from *Pseudomonas aeruginosa*. *Microbiol Immunol* 49:999–1002.
2. Mima T, Joshi S, Gomez-Escalada M, Schweizer HP (2007) Identification and characterization of TriABC-OpmH, a triclosan efflux pump of *Pseudomonas aeruginosa* requiring two membrane fusion proteins. *J Bacteriol* 189:7600–7609.
3. Poole K, Srikumar R (2001) Multidrug efflux in. *Pseudomonas aeruginosa*: Components, mechanisms, and clinical significance. *Curr Top Med Chem* 1:59–71.
4. Seeger MA, *et al.* (2006) Structural asymmetry of AcrB trimer suggests a peristaltic pump mechanism. *Science* 313:1295–1298.
5. Murakami S, Nakashima R, Yamashita E, Matsumoto T, Yamaguchi A (2006) Crystal structures of a multidrug transporter reveal a functionally rotating mechanism. *Nature* 443:173–179.
6. Muller JF, Stevens AM, Craig J, Love NG (2007) Transcriptome analysis reveals that multidrug efflux genes are up-regulated to protect *Pseudomonas aeruginosa* from pentachlorophenol stress. *Appl Environ Microbiol* 73:4550–4558.
7. Saito K, Yoneyama H, Nakae T (1999) *nalB*-type mutations causing the overexpression of the MexAB-OprM efflux pump are located in the mexR gene of the *Pseudomonas aeruginosa* chromosome. *FEMS Microbiol Lett* 179:67–72.
8. Srikumar R, Paul CJ, Poole K (2000) Influence of mutations in the *mexR* repressor gene on expression of the MexA-MexB-oprM multidrug efflux system of *Pseudomonas aeruginosa*. *J Bacteriol* 182:1410–1414.
9. Cao L, Srikumar R, Poole K (2004) MexAB-OprM hyperexpression in NalC-type multidrug-resistant *Pseudomonas aeruginosa*: Identification and characterization of the *nalC* gene encoding a repressor of PA3720-PA3719. *Mol Microbiol* 53:1423–1436.
10. Llanes C, *et al.* (2004) Clinical strains of *Pseudomonas aeruginosa* overproducing MexAB-OprM and MexXY efflux pumps simultaneously. *Antimicrob Agents Chemother* 48:1797–1802.
11. Sobel ML, Hocquet D, Cao L, Plesiat P, Poole K (2005) Mutations in. *PA3574* (*nalD*) lead to increased MexAB-OprM expression and multidrug resistance in laboratory and clinical isolates of *Pseudomonas aeruginosa*. *Antimicrob Agents Chemother* 49:1782–1786.
12. Boutoille D, *et al.* (2004) Detection of an IS21 insertion sequence in the *mexR* gene of *Pseudomonas aeruginosa* increasing $\beta$-lactam resistance. *FEMS Microbiol Lett* 230:143–146.
13. Morita Y, Cao L, Gould VC, Avison MB, Poole K (2006) *nalD* encodes a second repressor of the *mexAB-oprM* multidrug efflux operon of *Pseudomonas aeruginosa*. *J Bacteriol* 188:8649–8654.
14. Evans K, Adewoye L, Poole K (2001) MexR repressor of the. *mexAB-oprM* multidrug efflux operon of *Pseudomonas aeruginosa*: Identification of MexR binding sites in the *mexA-mexR* intergenic region. *J Bacteriol* 183:807–812.
15. Saito K, Eda S, Maseda H, Nakae T (2001) Molecular mechanism of MexR-mediated regulation of MexAB-OprM efflux pump expression in *Pseudomonas aeruginosa*. *FEMS Microbiol Lett* 195:23–28.
16. Daigle DM, *et al.* (2007) A protein modulator of multidrug efflux gene expression in *Pseudomonas aeruginosa*. *J Bacteriol* 189:5441–5451.
17. Wilkinson SP, Grove A (2006) Ligand-responsive transcriptional regulation by members of the MarR family of winged helix proteins. *Curr Issues Mol Biol* 8:51–62.
18. Ellison DW, Miller VL (2006) Regulation of virulence by members of the MarR/SlyA family. *Curr Opin Microbiol* 9:153–159.
19. Alekshun MN, Levy SB, Mealy TR, Seaton BA, Head JF (2001) The crystal structure of MarR, a regulator of multiple antibiotic resistance, at 2.3-A resolution. *Nat Struct Biol* 8:710–714.
20. Newberry KJ, Fuangthong M, Panmanee W, Mongkolsuk S, Brennan RG (2007) Structural mechanism of organic hydroperoxide induction of the transcription regulator OhrR. *Mol Cell* 28:652–664.
21. Bordelon T, Wilkinson SP, Grove A, Newcomer ME (2006) The crystal structure of the transcriptional regulator HucR from *Deinococcus radiodurans* reveals a repressor preconfigured for DNA binding. *J Mol Biol* 360:168–177.
22. Kumarevel T, *et al.* (2008) Crystal structure of the MarR family regulatory protein, ST1710, from *Sulfolobus tokodaii* strain 7. *J Struct Biol* 161:9–17.
23. Hong M, Fuangthong M, Helmann JD, Brennan RG (2005) Structure of an OhrR-ohrA operator complex reveals the DNA binding mechanism of the MarR family. *Mol Cell* 20:131–141.
24. Saridakis V, Shahinas D, Xu X, Christendat D (2008) Structural insight on the mechanism of regulation of the MarR family of proteins: High-resolution crystal structure of a transcriptional repressor from *Methanobacterium thermoautotrophicum*. *J Mol Biol* 377:655–667.
25. Lim D, Poole K, Strynadka NC (2002) Crystal structure of the MexR repressor of the. *mexRAB-oprM* multidrug efflux operon of *Pseudomonas aeruginosa*. *J Biol Chem* 277:29253–29259.
26. Yamada H, *et al.* (2007) ''Crystal lattice engineering,'' an approach to engineer protein crystal contacts by creating intermolecular symmetry: Crystallization and structure determination of a mutant human RNase 1 with a hydrophobic interface of leucines. *Protein Sci* 16:1389–1397.
27. Baumgarth B, Bartels FW, Anselmetti D, Becker A, Ros R (2005) Detailed studies of the binding mechanism of the *Sinorhizobium meliloti* transcriptional activator ExpG to DNA. *Microbiology* 151:259–268.
28. Wilkinson SP, Grove A (2005) Negative cooperativity of uric acid binding to the transcriptional regulator HucR from *Deinococcus radiodurans*. *J Mol Biol* 350:617–630.
29. Saito K, Akama H, Yoshihara E, Nakae T (2003) Mutations affecting DNA-binding activity of the MexR repressor of *mexR-mexA-mexB-oprM* operon expression. *J Bacteriol* 185:6195–6198.
30. Chen PR, *et al.* (2006) An oxidation-sensing mechanism is used by the global regulator MgrA in *Staphylococcus aureus*. *Nat Chem Biol* 2:591–595.
31. Lee JW, Soonsanga S, Helmann JD (2007) A complex thiolate switch regulates the *Bacillus subtilis* organic peroxide sensor OhrR. *Proc Natl Acad Sci USA* 104:8743–8748.
32. Soonsanga S, Lee JW, Helmann JD (2008) Oxidant-dependent switching between reversible and sacrificial oxidation pathways for *Bacillus subtilis* OhrR. *Mol Microbiol* 20:131–141.
33. Pace CN, Vajdos F, Fee L, Grimsley G, Gray T (1995) How to measure and predict the molar absorption coefficient of a protein. *Protein Sci* 4:2411–2423.
34. Otwinowski Z, Minor W (1997) Processing of x-ray diffraction data collected in oscillation mode. *Methods Enzymol* 276:307–326.
35. McCoy AJ, *et al.* (2007) Phaser crystallographic software. *J App Crystallgr* 40:658–674.
36. Vagin AA, Teplyakov A (1997) MOLREP: An automated program for molecular replacement. *J Appl Crystallgr* 30:1022–1025.
37. Emsley P, Cowtan K (2004) Coot: Model-building tools for molecular graphics. *Acta Crystallogr D* 60:2126–2132.
38. Adams PD, *et al.* (2002) PHENIX: Building new software for automated crystallographic structure determination. *Acta Crystallogr D* 58:1948–1954.
39. Collaborative Computational Project No. 4 (1994) The CCP4 suite programs for protein crystallography. *Acta Crystallogr D* 50:760–763.
40. DeLano WL (2002) The PyMOL Molecular Graphics System (DeLano Scientific, San Carlos, CA).
41. Pettersen EF, *et al.* (2004) UCSF Chimera: A visualization system for exploratory research and analysis. *J Comput Chem* 25:1605–1612.